

CATHENA VALIDATION AGAINST MAPLE SUBCOOLED BOILING DATA

T.V. TRAN, S.Y. SHIM, J.E. KOWALSKI and M. SALCUDEAN

AECL Research
Whiteshell Laboratories
Pinawa, Manitoba R0E 1L0

ABSTRACT

The MAPLE-X10 (Multipurpose Applied Physics Lattice Experimental-NRX 10 MW) reactor developed by AECL Research [1] is a light-water-cooled pool-type reactor. The reactor is currently being built at AECL's Chalk River Laboratories, and will be used as a dedicated isotope producer. The non-equilibrium effects of subcooled boiling are predicted to strongly affect the transient behaviour of the reactor under some postulated upset conditions in MAPLE-X10. It is necessary to be able to predict the local subcooled void fraction accurately to be able to determine the core pressure drop, the mass flux and void reactivity effects.

CATHENA, an advanced two-fluid thermalhydraulics code [2,3], was used to predict the void fractions during subcooled boiling for conditions measured in the MAPLE single-pin heat transfer test facilities at AECL's Whiteshell Laboratories (WL) and at the University of British Columbia (UBC). Subcooled boiling void fractions must be predicted accurately by CATHENA, especially if the code is intended to simulate the void-reactivity feedback effect on power in the MAPLE-X10 reactor. The data provide void fractions measured at a fixed location near the top of the Fuel Element Simulator (FES) for high flows (WL) and for low flows (UBC). These data cover pressures between 110 and 328 kPa, local subcoolings between 8 and 86°C, and flow velocities from 0.1 to 6.0 m/s. Good agreement was obtained with CATHENA void fraction calculations for the majority of the cases analyzed.

1.0 INTRODUCTION

In a light-water-cooled reactor such as the MAPLE-X10, the coolant is predicted to boil in the high heat flux under some postulated accident conditions. Before bulk boiling begins, a

condition exists where the local temperature of the heated surface exceeds the local liquid saturation temperature, and the bulk liquid temperature is less than its local saturation temperature. Under this condition, heat transfer to the liquid raises the liquid temperature adjacent to the heated surface to its saturation temperature, causing local vapour to be generated. This non-equilibrium phenomenon is referred to as subcooled boiling. Griffith et al. [4] pointed out that there are two distinct subcooled regions: (1) the wall void region, and (2) the detached void region.

Many subcooled boiling void models were identified in a literature survey, but none was suitable for the MAPLE-X10 finned-fuel pin geometries and operating conditions. Chatoorgoon et al. [5] reviewed the existing subcooled boiling void models. Their work presented three levels of generation-condensation void models: (1) the exponential model, (2) the mechanistic model and (3) the thermal non-equilibrium model. CATHENA uses a subcooled void model developed for MAPLE-X10 finned-fuel pin geometries and operating conditions based on the two-fluid non-homogeneous and non-equilibrium approach.

This paper will briefly describe: the experiments performed at WL and UBC, the subcooled boiling void model used in CATHENA to calculate the void fraction, the parameters that affect the CATHENA void fraction calculation, and the comparison of simulation results with experimental data.

2.0 DESCRIPTION OF EXPERIMENTS

2.1 Experimental Conditions

Experiments performed at WL and UBC cover the range of conditions expected for the MAPLE-X10 reactor under postulated upset and accident conditions. Table 1 shows the range of

conditions for both the WL and UBC experiments.

The experimental results from WL and UBC served as the basis for the comparisons in this paper. Experiments performed at UBC were conducted at velocities between 0.12 and 1.10 m/s whereas the experiments at WL were conducted at velocities between 0.9 and 6.0 m/s. The data in the overlap region between the two velocity ranges were compared against each other for consistency.

TABLE 1

WL AND UBC EXPERIMENTAL CONDITIONS

Conditions	UBC	WL
Coolant Velocities (m/s)	0.12-1.10	0.90-6.00
Local Subcoolings (°C)	8.0-60.0	27.5-65.5
Inlet Pressures (kPa)	110-300	118-328
Heat Flux (MW/m ²)	0.26-1.57	1.30-7.67
Hydraulic Diameters (mm)	5.37-7.30	5.37-13.66
Heated Diameters (mm)	10.55-16.76	10.55-38.64

2.2 Test Facilities

The heat transfer test section at UBC is similar to the facility located at WL. The procedures used to conduct the experiments at WL and UBC are also similar. Therefore only the WL test facility will be described.

Figure 1 shows a schematic flow diagram of the MAPLE-X10 single-pin heat transfer test facility. The experimental apparatus consists of a surge tank, two heat exchangers, a flow-circulation pump driven by a variable-speed motor, the test section, and interconnecting pipes. The test section is made from glass tubing to allow direct visual observation of the heat transfer phenomena. The 17-mm and 24-mm I.D. glass tubes were used to investigate the effect of the hydraulic diameter on the heat transfer rate.

2.3 Test Section

A Fuel Element Simulator (FES) is located inside

the glass tube. The total length of the FES is 0.62 m, including a 0.02-m adiabatic brass section at both ends of the FES. The FES is made from a thin-walled stainless steel tube coated with aluminum oxide and clad with an outer aluminum sheath having either eight or ten longitudinal, rectangular fins. The axial power distribution along the length of the FES is uniform. The FES surface geometry is identical to the actual driver 8-fin and Moly 10-fin fuel pins used in the MAPLE-X10 reactor. Figure 2 shows both heaters with their dimensions. Heat was generated in the test section by directly heating the stainless steel tube from a stabilized DC power supply.

2.4 Experimental Measurements

The following parameters, most shown in Figure 1, were measured in each experiment:

- The average cross-sectional void fraction was measured at a single location by a single-beam gamma densitometer. The gamma densitometer was located 5.0 cm upstream of the end of heated portion of the FES.
- The flow rate (F) was measured by a turbine flow meter.
- The bulk coolant (T_b), sheath (T_{sh}) and fin tip (T_{ft}) temperatures were measured by K-type thermocouples.
- The inlet and outlet coolant temperatures (T) were monitored by resistance temperature detectors.
- The absolute inlet and outlet pressures (P) along with the pressure drops at each third of the heated section were measured using Rosemount differential pressure transmitters.
- The power input was calculated from the voltage and current measured at the heater.

In addition, the Onset of Nucleate Boiling (ONB) and the Onset of Significant Void (OSV) points were determined during each experiment by visual observations and with the aid of a strobe light.

2.5 Experimental Procedure

Before each experiment was performed, the water was thoroughly degassed to purge the noncondensable gases so that they would not affect the heat transfer study. The inlet temperature, pressure and coolant flow rate were kept constant

during each void fraction experiment. The input power was the only parameter varied.

3.0 EXISTING VOID MODELS IN CATHENA

Two void models already existed in CATHENA when development work began on a subcooled boiling void model for the MAPLE-X10: the liquid superheated hyperbolic tangent void model and the Hancox and Nicoll void model [6]. Because the Hancox and Nicoll void model is more physically based it was assessed for prediction of MAPLE-X10 type conditions. Based on an initial assessment, it was decided to implement the MAPLE-X10 subcooled boiling void model within the CATHENA code.

Figures 3 and 4 compare the predictions of the subcooled void profile using the Hancox and Nicoll void model and the MAPLE-X10 subcooled boiling void model at high flow rates and low flow rates respectively. For the high-flow-rate experiment shown in Figure 3, the Hancox and Nicoll void model predicted no void fraction until the input power reached 114.3 kW, whereas the MAPLE-X10 subcooled boiling void model predicted void fraction in better agreement with the experimental data. Figure 3 shows that the Hancox and Nicoll void model overestimated the power to obtain the initial point of net void generation. For the low-flow-rate experiment, the MAPLE-X10 subcooled boiling void model and the Hancox and Nicoll void model predicted a similar void profile beyond the OSV point, as shown in Figure 4. It is noted that the Hancox and Nicoll void model does not consider any wall-void region. Based on this investigation, the Hancox and Nicoll void model was considered to be inadequate for MAPLE-X10 conditions.

Subcooled boiling void models that are formulated for the high-pressure conditions typical of power reactors are generally not directly applicable to low pressures. This fact has been confirmed by Evangelisti and Lupoli [7]. The need to develop a better void model for MAPLE-X10 conditions prompted the current work.

4.0 MAPLE-X10 SUBCOOLED BOILING VOID MODEL

The MAPLE-X10 subcooled boiling void model used in CATHENA includes both regions of subcooled boiling: the region between ONB and OSV (the wall-void region) and the region beyond OSV (the detached-void region). The OSV point

serves as an intersection between the wall-void and the detached-void regions. The OSV point was determined graphically by plotting the experimental void characteristic profile, as illustrated in Figure 5. The slope of the void profile in the detached-void region is significantly higher than the slope of the void profile in the wall-void region.

The void fraction is modelled mechanistically beyond the OSV point (detached-void region). However, the void calculation in the wall-void region is determined by a simple correlation derived from the same data base that was used to develop the OSV correlation. The wall-void correlation is described below.

4.1 Wall-Void Correlation

The wall-void correlation describes the thickness of the bubble boundary layer under which bubbles may be generated. When the surface heat flux is below the ONB heat flux, no bubble formation is calculated and all the heat flux from the heated surface is transferred to the subcooled liquid. The coolant flows as a single-phase liquid. When the surface heat flux exceeds the ONB heat flux, but remains below the OSV heat flux, bubbles start to form on the heated surface. The majority of these bubbles collapse immediately because of intensive condensation, but some of these bubbles will remain attached to or slide along the heated surface. The formation of the wall void in this region is computed by linear interpolation between the two limiting ONB and OSV fluxes:

$$\alpha_w = 0.0 \quad \text{for } \dot{q} \leq \dot{q}_{ONB} \quad (1)$$

$$\alpha_w = \alpha_{OSV} \cdot FR \quad \text{for } \dot{q}_{ONB} < \dot{q} \leq \dot{q}_{OSV} \quad (2)$$

where

$$FR = (\dot{q} - \dot{q}_{ONB}) / (\dot{q}_{OSV} - \dot{q}_{ONB})$$

$$\dot{q} = \text{heat flux from the wall surface (W/m}^2\text{)}$$

$$\dot{q}_{ONB} = \text{ONB heat flux (W/m}^2\text{)}$$

$$\dot{q}_{OSV} = \text{OSV heat flux (W/m}^2\text{)}$$

$$\alpha_w = \text{void fraction in the wall-void region}$$

$$\alpha_{OSV} = \text{void fraction at the OSV heat flux.}$$

α_{OSV} was developed from the same data base that was used to develop the OSV correlation. Rogers et al. [8] measured α_{OSV} to be up to 10% for

low-subcooling and low-flow conditions. Rouhani [9] derived the following expression for α_{OSV} :

$$\alpha_{OSV} = \delta \cdot P_h / A \quad (3)$$

where

$\delta \approx 0.67 \cdot r_d \approx 0.002435 \cdot P^{-0.237}$, the average vapour thickness on the wall (m)

P_h = heated perimeter (m)

A = cross-sectional flow area (m^2)

P = pressure (N/m^2)

r_d = average bubble radius at departure point (m).

Rouhani derived Equation (3) for pressures between 0.1 and 10 MPa. Evangelisti et al. made a similar derivation [7]. Koumoutsos showed that the bubble size at OSV decreases with increasing velocity [10]. Based on the literature and the analysis of the available MAPLE-X10 data, the MAPLE-X10 α_{OSV} appears to depend primarily on three parameters: the geometry, the local subcooling of the coolant liquid, and its velocity. The MAPLE-X10 α_{OSV} correlation is given as:

$$\alpha_{OSV} = 0.01873 \cdot FNC \quad (4)$$

where

$$FNC = Re_b^{0.014} \cdot N_s^{0.212} \cdot A_r^{0.642} \cdot P_r^{0.899}$$

$Re_b = G \cdot D_h / \mu$, the Reynolds number evaluated at local bulk conditions

$N_s = \text{maximum}(-x_{eq}, 0.005)$

x_{eq} = thermal equilibrium quality $[(h-h_{sat})/h_{fg}]$

A_r = ratio of the cross-sectional flow area per pin to the reference cross-sectional flow area

P_r = ratio of the fuel pin cross-sectional area to the reference fuel pin cross-sectional area.

Figure 6 compares the MAPLE-X10 α_{OSV} correlation with the experimental data. The root mean square (RMS) error is $\pm 47\%$. The error was caused mainly because of the difficulty of measuring such a low void fraction with high accuracy. Because of this uncertainty the wall-void fraction is reduced to a half of the α_{OSV}

calculated by Equation (4) when implemented in CATHENA. The void generated in the wall-void region was assumed to have no effect on the thermalhydraulics calculations. However, the wall void is used in the reactor kinetics calculation. By reducing the value of the wall void by a half, the reactor power increase due to less negative reactivity feedback in the reactor kinetics modelling, results in a power calculation that is conservative.

The void fraction computed in the detached-void region is the net result of two competing mechanisms: void generation and condensation. Sections 4.2 and 4.3 briefly describes how CATHENA models the void generation and condensation components, respectively.

4.2 Void Generation

The void generation component in CATHENA is modelled through the amount of heat partitioned between vapour generation and heating the subcooled liquid. The heat flux obtained from the OSV correlation is used as the amount of heat flux going into the subcooled liquid to raise the liquid temperature while the remainder (difference between the heat flux from the heated surface and the OSV heat flux) goes into generating the void.

The void generation is a direct function of the splitting factor (FB). The splitting factor is defined as the fraction of the wall heat flux transferred to the subcooled liquid. The remainder $(1.0 - FB)$ contributes to vapour generation. The splitting fraction calculated in the CATHENA subcooled void model is given below.

$$FB = 1.0 \quad \text{for } \dot{q} \leq \dot{q}_{OSV} \quad (5)$$

$$FB = \dot{q}_{OSV} / \dot{q} \quad \text{for } \dot{q} > \dot{q}_{OSV} \quad (6)$$

4.3 Void Condensation

The CATHENA condensation rate is a strong function of the interfacial (liquid to vapour) heat transfer coefficient, which in turn depends on the interfacial area per unit volume. This depends on the bubble size and its relative velocity.

The bubble size is a rather sensitive parameter in calculating the condensation rate, and so will ultimately affect the void calculation. The bubble diameter calculated by Wallis [11] was used in the CATHENA condensation model for the void

fraction region ($>1.0\%$), while a fixed bubble number, N_b , was used to calculate the bubble size in the void-fraction region below 1.0% . The bubble number, N_b , is determined so that the bubble diameter is continuous at the transition into the liquid phase. In addition, the maximum bubble diameter is limited to 20% of the equivalent hydraulic diameter. The bubble diameter relationship was chosen to avoid potential instabilities and to represent bubbly flow which was observed in the experiments. Because of this limit and the small hydraulic diameter in these experiments, 20% of the equivalent hydraulic diameter is used as the bubble diameter for all the cases simulated.

5.0 SENSITIVITY ANALYSIS

A sensitivity analysis of parameters affecting the void generation and condensation components in CATHENA has been investigated. The calculation of the void generation component in CATHENA, as mentioned earlier, depends primarily on which OSV model is selected. Many parameters in the CATHENA condensation model will affect the condensation calculation, but the most sensitive parameter is the bubble diameter. A high-flow-rate experiment and a low-flow-rate experiment were thus simulated using different OSV models and bubble diameters for this sensitivity study.

5.1 OSV Models

The models proposed by Rogers et al. [8], Saha and Zuber [12], and Hancox and Nicoll [6] were examined in the sensitivity study. The Rogers et al. model was formulated for conditions of low subcooling, low pressure range, and low coolant velocity; the Rogers et al. model was formulated for unfinned data similar to that used in the Saha and Zuber model for OSV. On the other hand, the Hancox and Nicoll model was formulated for high-pressure conditions. Figures 7 and 8 display the void fraction predictions of each model for the high-flow-rate and the low-flow-rate experiments. All three models underestimated the void fraction for both flow rates because the OSV point was predicted to occur at a higher power.

5.2 Bubble Diameter

As mentioned earlier, the bubble diameter used was 20% of the hydraulic diameter. In this sensitivity analysis, the bubble diameter is varied between 15% and 25% of the hydraulic diameter. Figures 9 and 10 show that the void fraction

increased as the bubble size increased. This indicates that the condensation rate calculated in CATHENA increases as the bubble diameter decreases.

6.0 SUMMARY AND DISCUSSION OF SIMULATION RESULTS

Table 2 summarizes all the simulated cases and the simulated conditions. However, the results of only a few selected experiments are compared with CATHENA predictions in this paper.

TABLE 2

SUMMARY TABLE OF SIMULATED EXPERIMENTS

Case Number	Fin Geometry	Inlet Press. (kPa)	Flow Rate (L/s)	Inlet Temp. ($^{\circ}\text{C}$)
1	8/WL	112.0	0.15	60.0
2	8/WL	145.0	0.50	40.0
3	8/WL	180.0	1.00	40.0
4	10/WL	180.0	0.60	60.0
5	10/WL	180.0	0.60	40.0
6	8/WL	224.0	0.15	25.0
7	8/WL	224.0	0.15	40.0
8	8/WL	220.0	0.15	60.0
9	8/WL	225.0	0.25	25.0
10	8/WL	222.0	0.25	40.0
11	8/WL	223.0	0.50	25.0
12	8/WL	223.0	0.50	40.0
13	8/WL	244.0	0.70	40.0
14	8/WL	234.0	1.00	40.0
15	10/WL	235.0	0.41	40.0
16	10/WL	272.0	0.60	40.0
17	8/WL	323.0	0.15	60.0
18	8/WL	325.0	0.50	40.0
19	10/WL	328.0	0.30	40.0
20	8/UBC	110.0	0.05	45.0
21	8/UBC	110.0	0.05	60.0
22	8/UBC	110.0	0.05	75.0
23	8/UBC	200.0	0.05	45.0
24	8/UBC	200.0	0.05	60.0
25	8/UBC	200.0	0.05	75.0
26	8/UBC	300.0	0.05	45.0
27	8/UBC	300.0	0.05	60.0
28	8/UBC	300.0	0.05	75.0

Figures 11 to 22 compare the void fraction calculations and experiments for the WL data and Figures 23 to 25 do the same for the UBC data. Only 8-fin experimental data from UBC were available, and they are included for comparison.

The input power versus void fraction are plotted for CATHENA calculations and compared with the experimental data. In general, the subcooled void fraction calculated by CATHENA is in good agreement with the experimental data.

The void fraction calculated in the wall-void region by the CATHENA code was generally lower than the experimental values. However, the code's predictions of the point of net vapour generation (the OSV point) and the amount of void fraction beyond the OSV point were in good agreement with the experimental data. It is important to predict the ONB and OSV points accurately because these points are used to determine the amount of void in the wall and detached regions. General observations on the CATHENA void calculations for WL and UBC data under various conditions are given in Sections 6.1 and 6.2.

6.1 WL Data

Void experiments were performed at various conditions for both geometries, driver 8-fin and Moly target 10-fin fuel pins. Most of the experiments were performed from single-phase flow until a critical heat flux (CHF) was reached or the fuel pin failed. Nineteen experimental cases covering various conditions and geometries were simulated as shown in Table 2. Twelve out of the nineteen experimental cases are reported in this paper.

The MAPLEX-10 subcooled boiling void model predicted the void fraction to within the measurement error of the experimental void fraction for inlet pressures between 110 and 180 kPa, as shown in Figures 11 to 14. For inlet pressures between 220 and 272 kPa, the void fractions calculated by the MAPLE-X10 subcooled boiling void model were also in good agreement with the experimental data for both regions of subcooling at various powers, subcoolings and flow rates, as shown in Figures 15 to 20. This agreement is attributed to the accurate prediction of the OSV point by the MAPLE OSV correlation.

Two 8-fin driver fuel experiments were simulated for pressures above 300 kPa. Figures 21 and 22 indicate that the CATHENA void predictions are in agreement with the experimental data.

6.2 UBC Data

In total, nine void experiments of 8-fin data from UBC were simulated for the comparison, as shown

in Table 2. Figures 23 to 25 compare the CATHENA predictions with experimental data for three of the nine experiments. In general, the MAPLE-X10 subcooled boiling void model predictions matched the experimental data well within the detached-void region, but slightly underestimated the results for the wall-void region.

7.0 CONCLUSIONS

Overall, the MAPLE-X10 subcooled boiling void model in the CATHENA code accurately captured the magnitude and the profile of net void generation well for the majority of the cases simulated. The following general conclusions are noted.

- The MAPLE-X10 subcooled boiling void model in the CATHENA code generally predicted slightly lower void fractions for low flow rates (flow rates < 0.9 m/s) and slightly overestimated the void fraction at higher flow rates in the detached-void region.
- Generally, the CATHENA code predicted the OSV point and the void fraction beyond the OSV point with better accuracy than models currently available in the literature.

ACKNOWLEDGEMENTS

The authors wish to thank Les Hembroff, Ken McCallum and Glenn Harvel for performing the experiments at WL, and Eric Bibeau for performing the experiments at UBC.

REFERENCES

1. LIDSTONE, R.F. and J.I. SAROUDIS, "MAPLE: A New Multipurpose Reactor for National Nuclear Development in the 1990s," Proc. of Int. Symposium on the Significance and Impact for Nuclear Research in Developing Countries, International Atomic Energy Agency, IAEA-SM-291/19 (1986).
2. RICHARDS D.J., HANNA B.N., HOBSON N. and ARDRON K.H., "CATHENA: A Two-Fluid Code for CANDU LOCA Analysis," Presented at the Third International Topical Meeting on Reactor Thermalhydraulics, Newport, R.I., USA, 1985 October 15-18.

3. HANNA B.N., HOBSON N., and RICHARDS D.J., "One-Step Semi-Implicit Method for Solving the Transient Two-Fluid Equations that is Non-Courant Limited," Presented at the 11th National Heat Transfer Conference, Denver, Co., August 1985.
4. GRIFFITH, P., J.A. CLARK and W.M. ROHSENOW, "Void Volumes in Subcooled Boiling Systems," American Society of Mechanical Engineers, Paper No. 58-HT-19 (1958).
5. CHATOORGOON, V., G.R. DIMMICK, M.B. CARVER, W.N. SELANDER and M. SHOUKRI, "Application of Void Generation and Condensation Models to Predict Subcooled Boiling data at Low Pressures," 5th CNS/ANS Int. Conference on Numerical Methods in Nuclear Engineering, Montreal, 1990.
6. HANCOX, W.T. and W.B. NICOLL, "A General Technique for the Prediction of Void Distributions in Non-Steady Two-Phase Forced Convection," Int. J. Heat Mass Transfer 14, 1377-1394 (1971).
7. EVANGELISTI, R. and P. LUPOLI, "The Void Fraction in an Annular Channel at Atmospheric Pressure," Int. J. Heat Mass Transfer 12, 699-711 (1969).
8. ROGERS, J.T., M. SALCUDEAN, Z. ABDULLAH, D. McLEOD and D. POIRIER, "The Onset of Significant Void in Up-Flow Boiling of Water at Low Pressures and Velocities," Int. J. Heat Mass Transfer 30, 2247-2260 (1987).
9. ROUHANI, S.Z., "Calculation of Steam Volume Fraction in Subcooled Boiling," J. Heat Transfer 90, 158-164 (1968).
10. KOUMOUTSOS, N., R. MOISSIS and A. SPYRIDONOS, "A Study of Bubble Departure in Forced-Convection Boiling," J. Heat Transfer 90, 223-230 (1968).
11. WALLIS, G.B., "One-Dimensional Two-Phase Flow," McGraw-Hill Book Publishing Co., New York, 1969.
12. SAHA, P. and N. ZUBER, "Point of Net Vapour Generation and Vapour Void Fraction in Subcooled Boiling," Proc. Fifth Int. Heat Transfer Conference, Volume IV, pp 175-179, Japan Society of Mechanical Engineering, Tokyo, 1974.

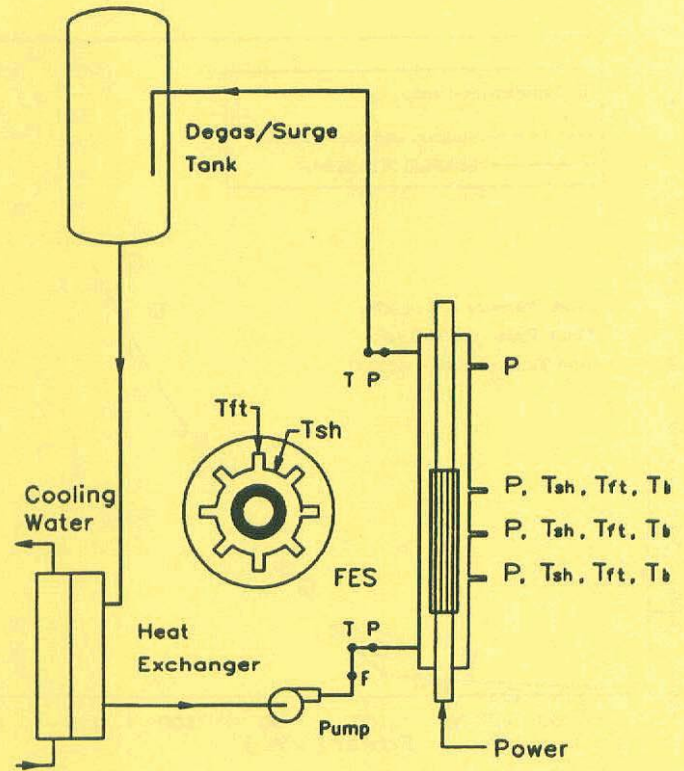
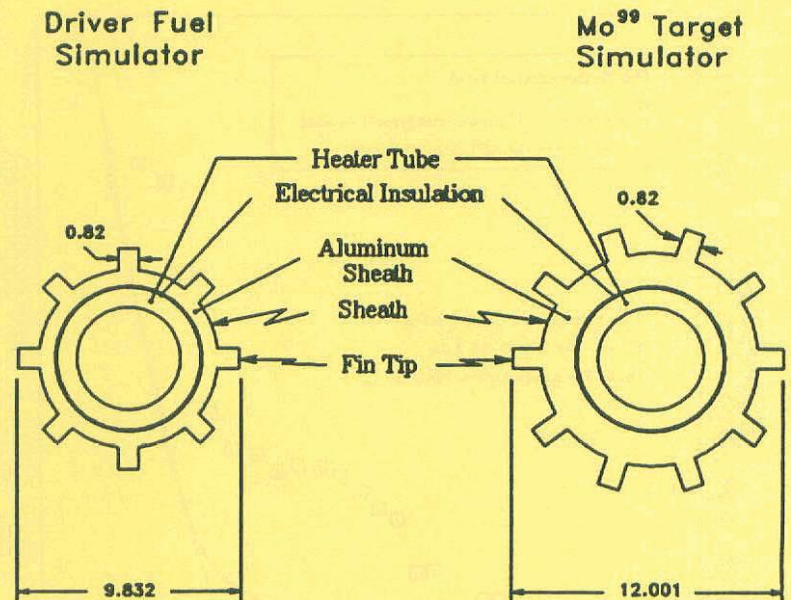


Fig. 1: Schematic Flow Diagram of the MAPLE-X10 Single-Pin Heat Transfer Test Facility at the Whiteshell Laboratories



Note: All dimensions in mm

Fig. 2: MAPLE-X10 Fuel Element Simulator (FES) Designs

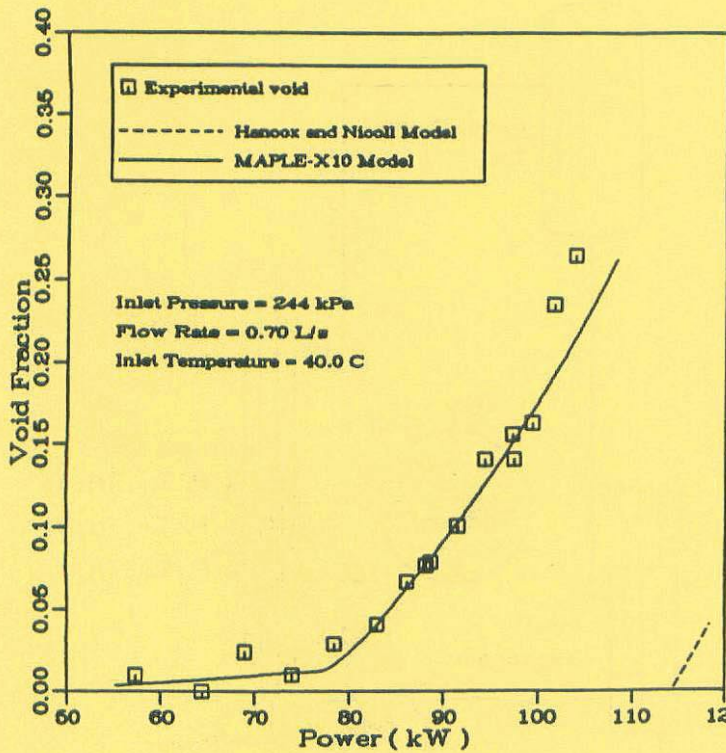


Fig. 3: Comparison between Hancox and Nicoll Void Model and MAPLE-X10 Void Model for the High-Flow-Rate Case

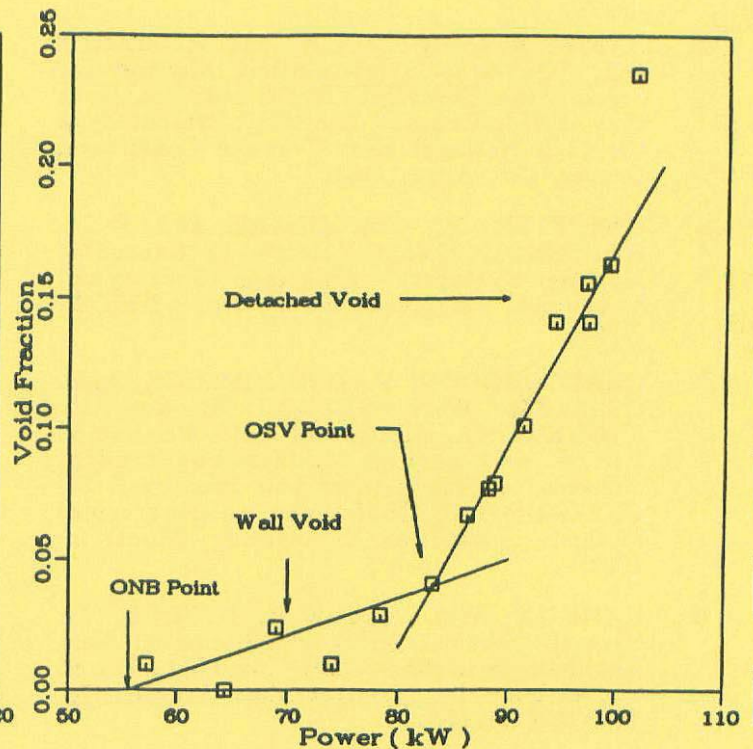


Fig. 5: Determination of OSV Point by Void Fraction Characteristics Profile

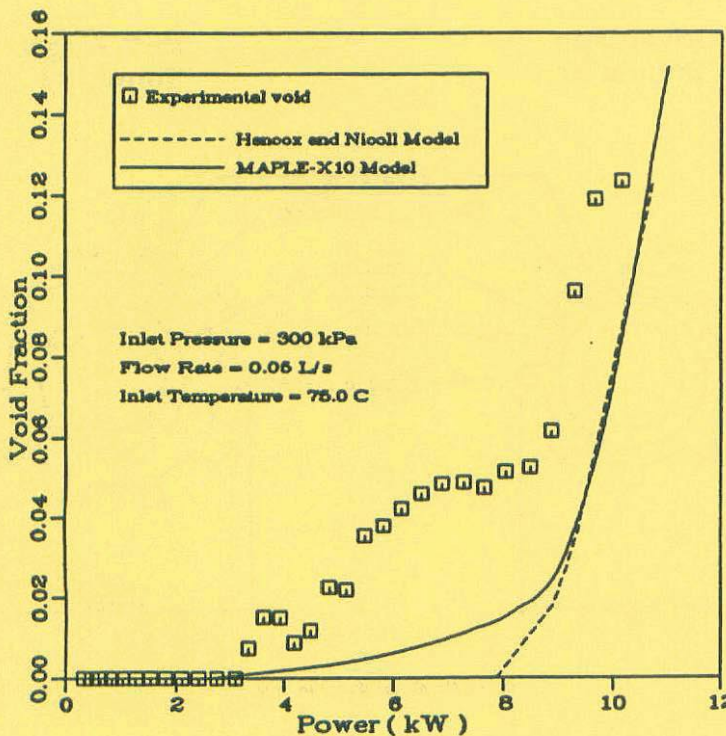


Fig. 4: Comparison between Hancox and Nicoll Void Model and MAPLE-X10 Void Model for the Low-Flow-Rate Case

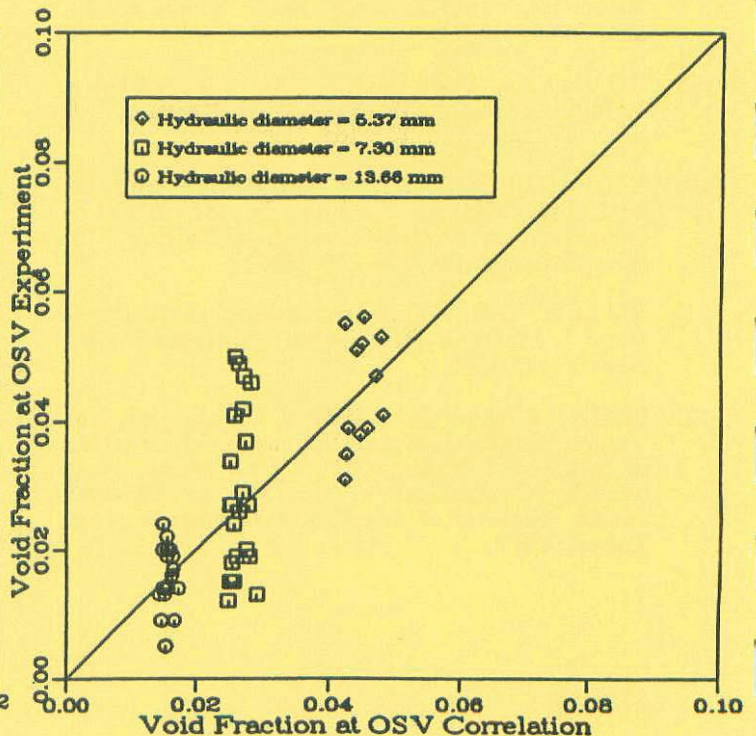


Fig. 6: MAPLE-X10 vs Correlation Against Experimental Data

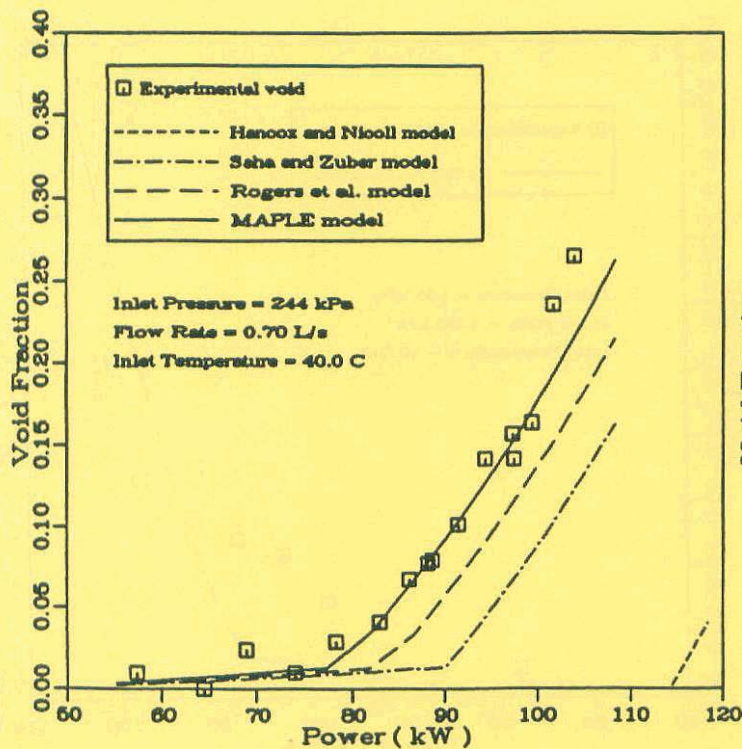


Fig. 7: Sensitivity Analysis of OSV Models for High-Flow-Rate Experiment

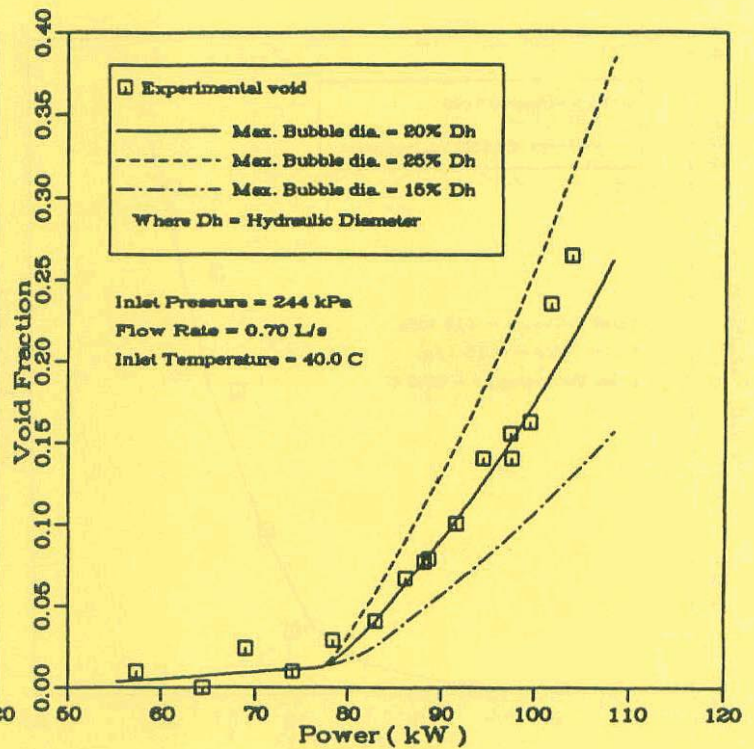


Fig. 9: Sensitivity Analysis of Bubble Diameter for High-Flow-Rate Experiment

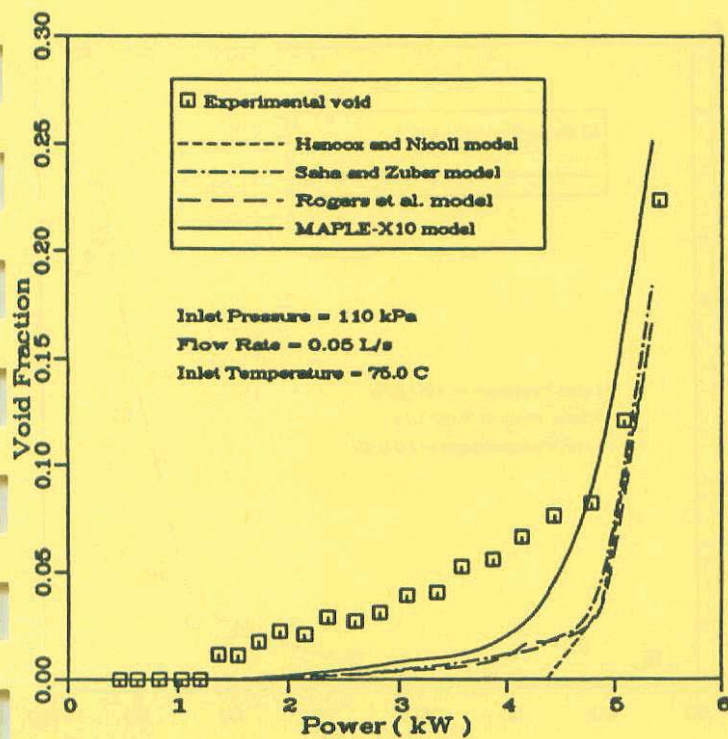


Fig. 8: Sensitivity Analysis of OSV Models for Low-Flow-Rate Experiment

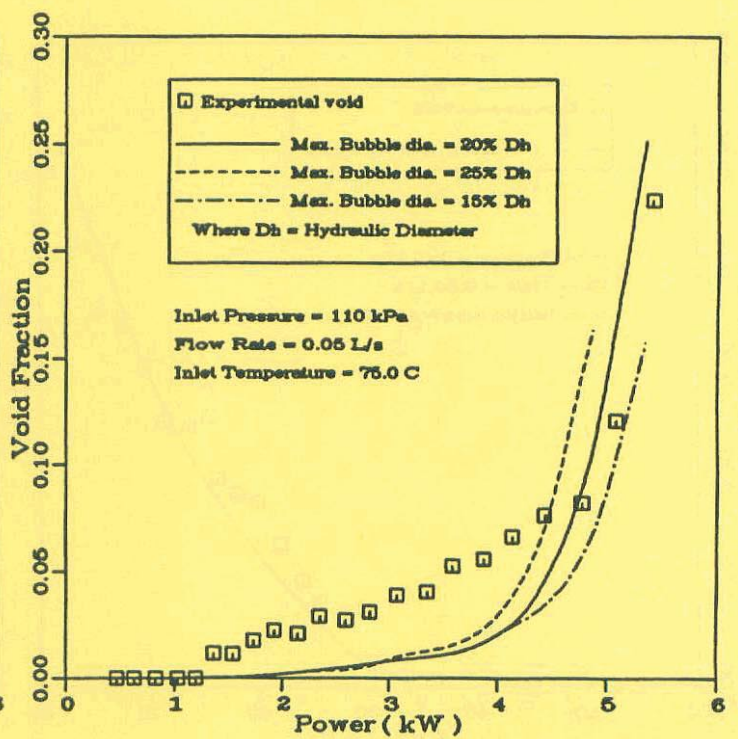


Fig. 10: Sensitivity Analysis of Bubble Diameter for Low-Flow-Rate Experiment

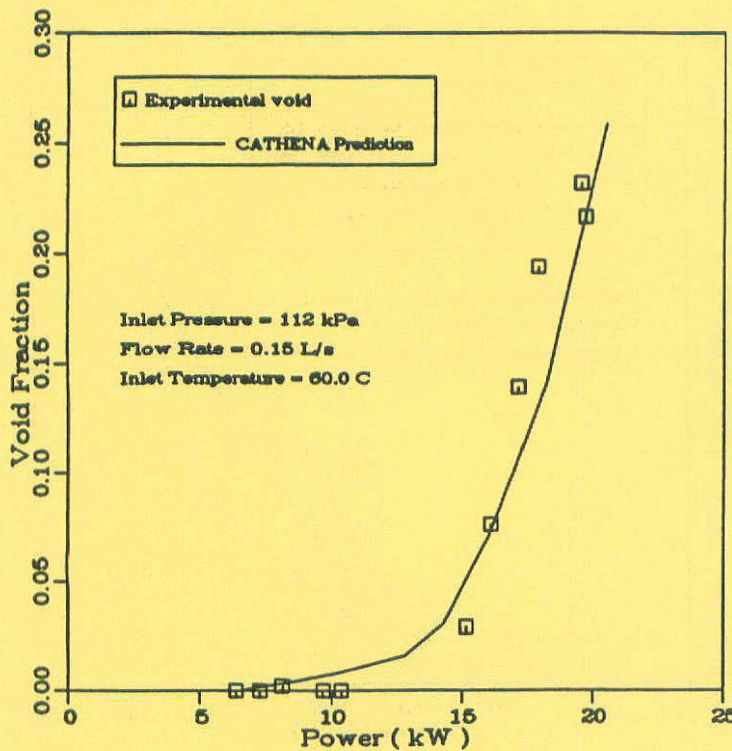


Fig. 11: CATHENA Prediction versus WL Experiment for 8-Fin Fuel

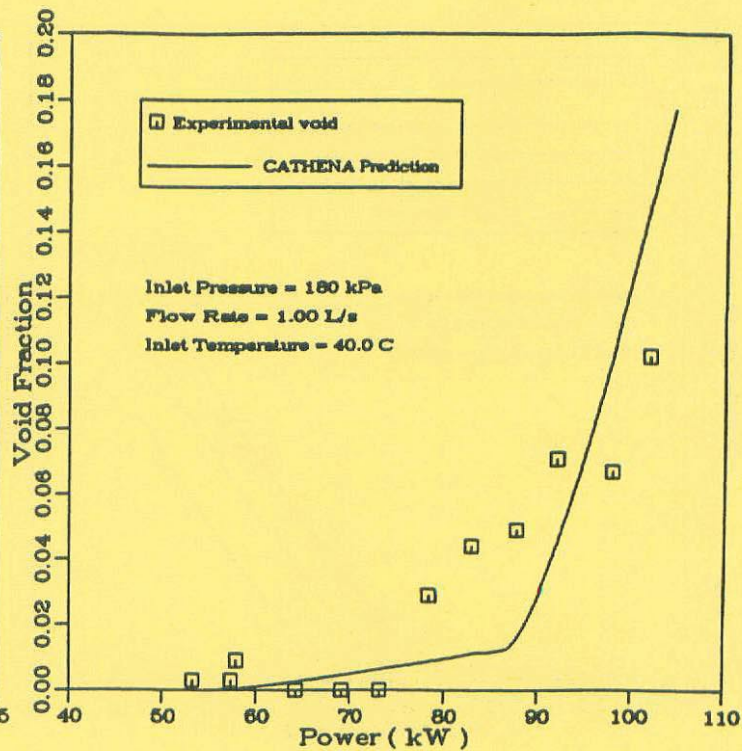


Fig. 13: CATHENA Prediction versus WL Experiment for 8-Fin Fuel

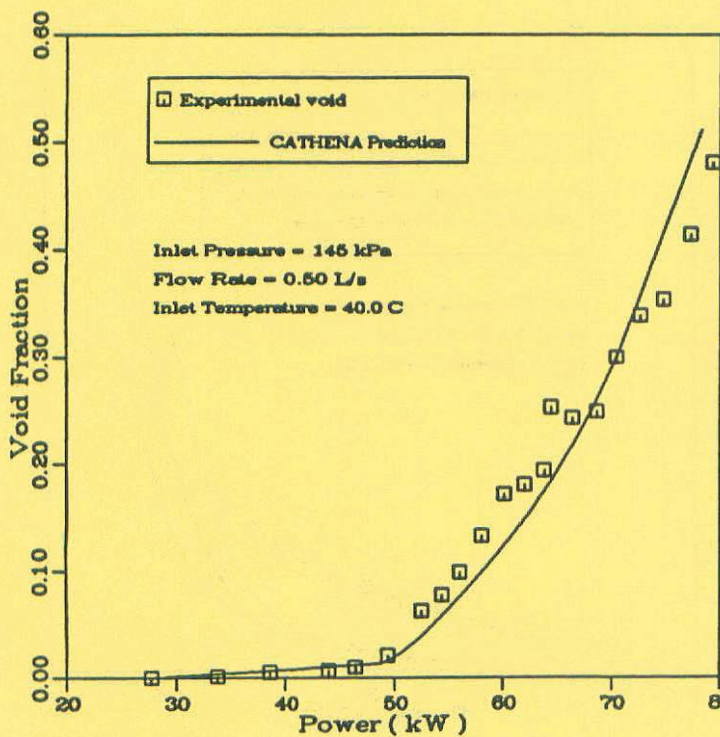


Fig. 12: CATHENA Prediction versus WL Experiment for 8-Fin Fuel

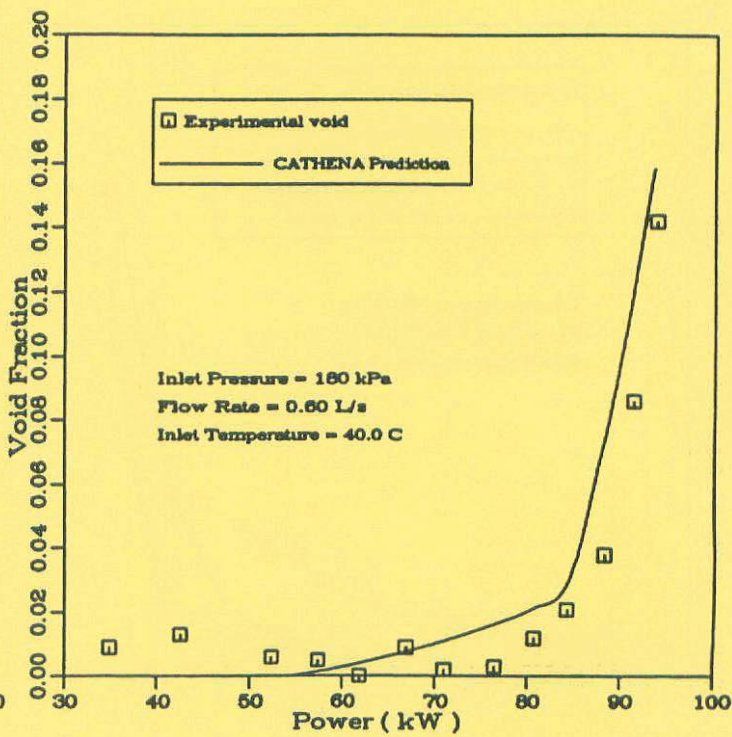


Fig. 14: CATHENA Prediction versus WL Experiment for 10-Fin Fuel

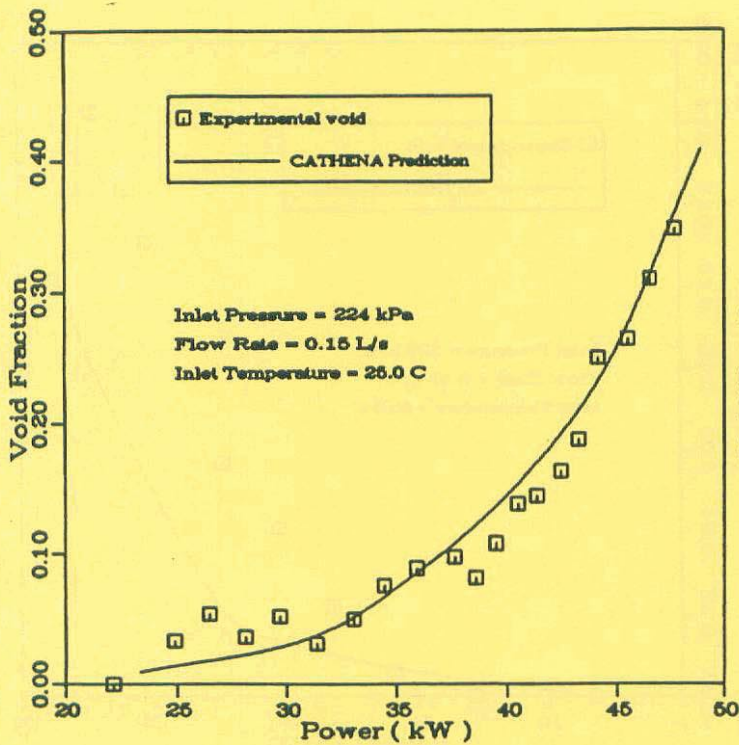


Fig. 15: CATHENA Prediction versus WL Experiment for 8-Fin Fuel

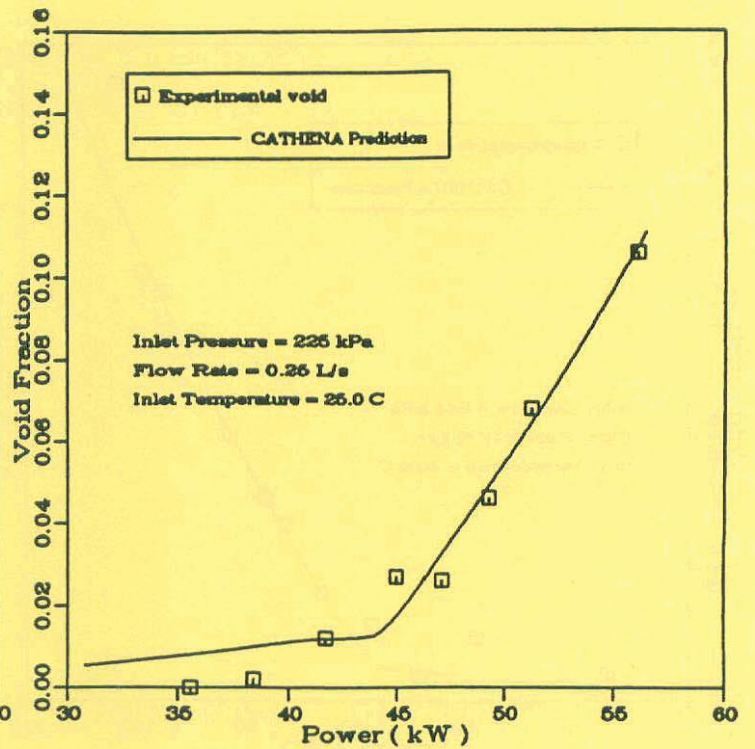


Fig. 17: CATHENA Prediction versus WL Experiment for 8-Fin Fuel

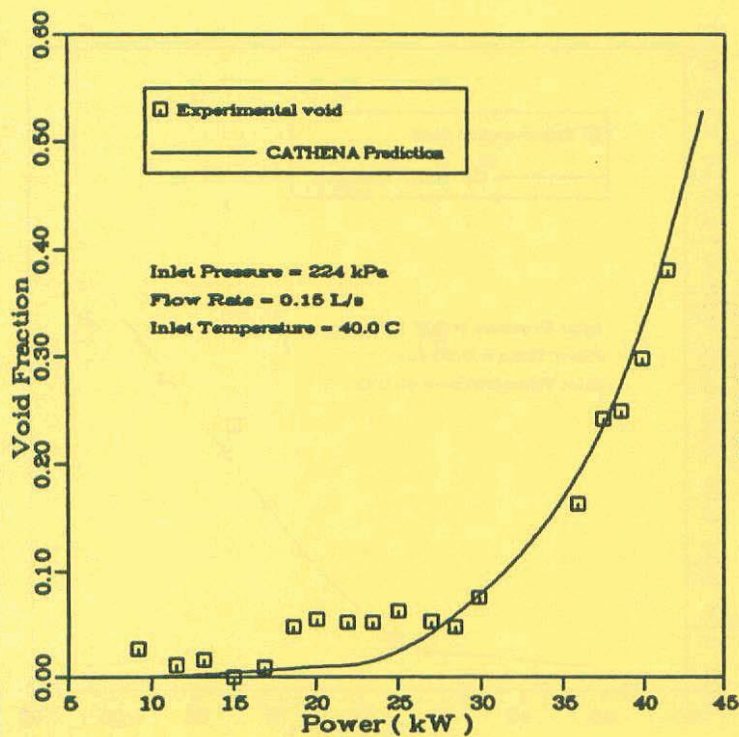


Fig. 16: CATHENA Prediction versus WL Experiment for 8-Fin Fuel

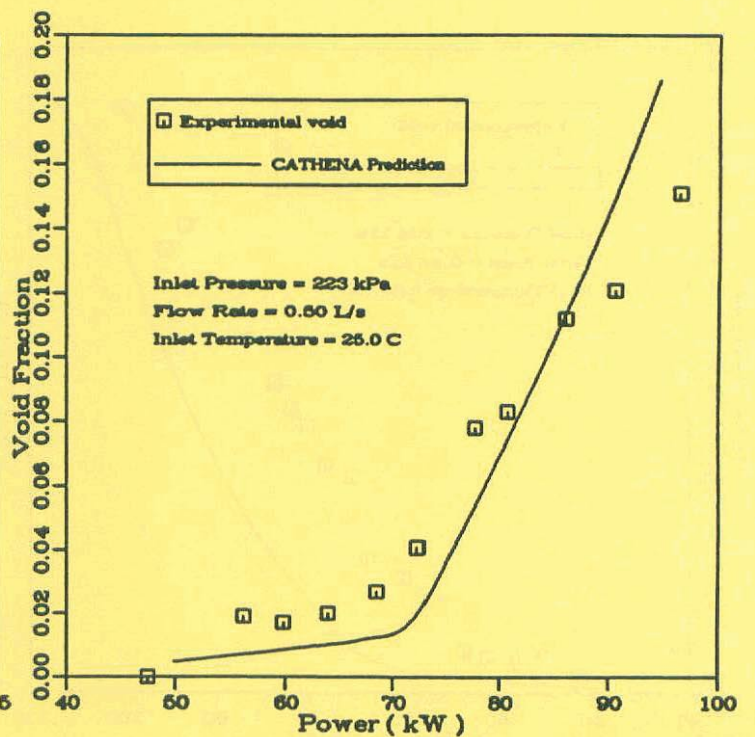


Fig. 18: CATHENA Prediction versus WL Experiment for 8-Fin Fuel

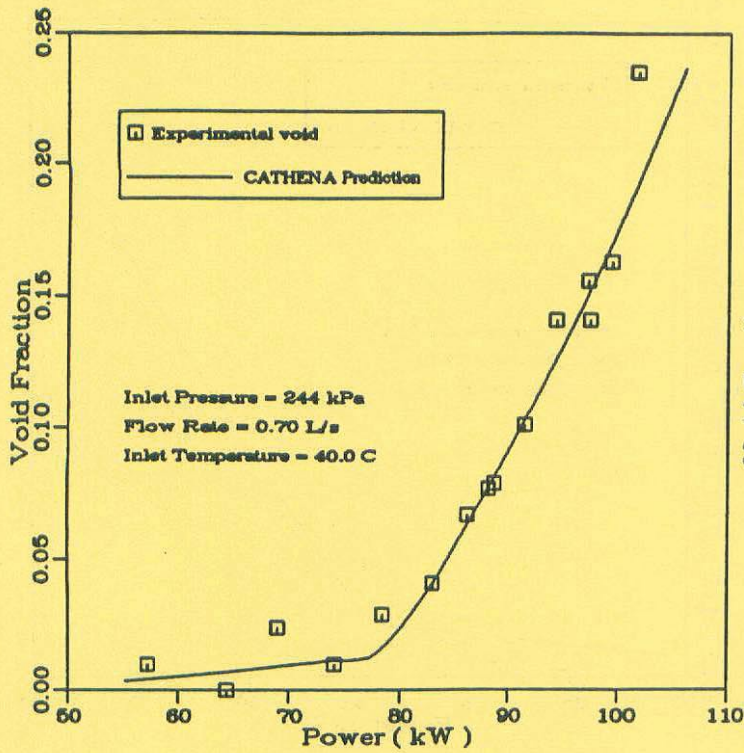


Fig. 19: CATHENA Prediction versus WL Experiment for 8-Fin Fuel

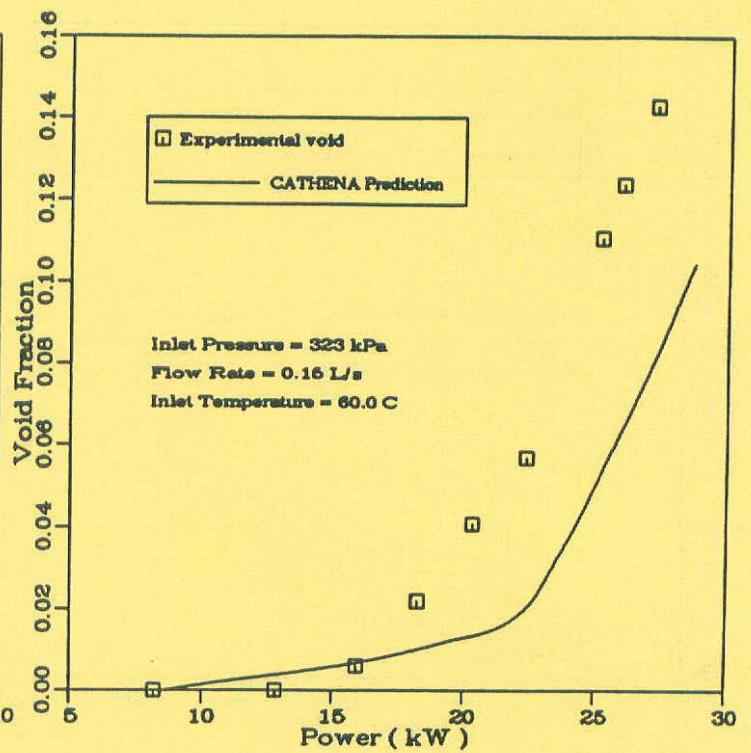


Fig. 21: CATHENA Prediction versus WL Experiment for 8-Fin Fuel

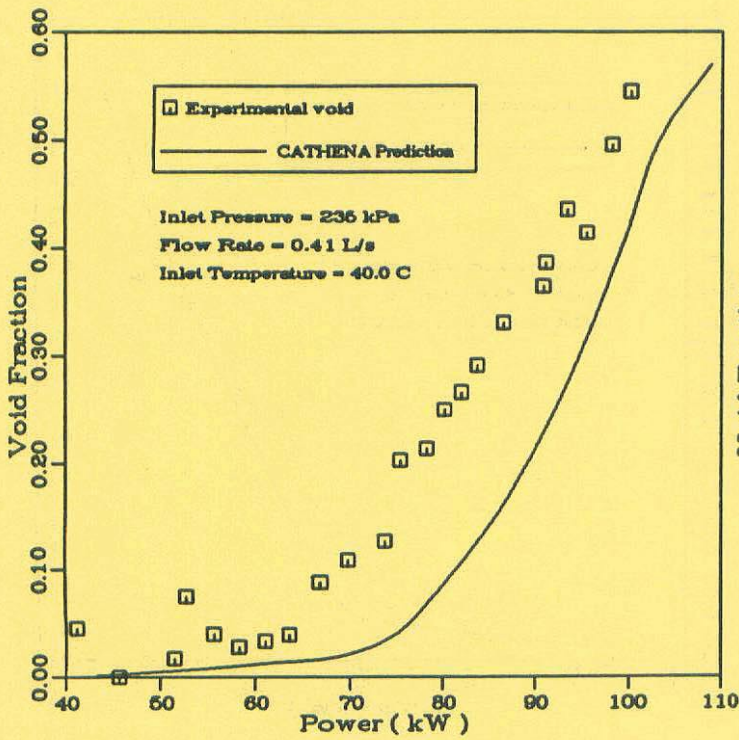


Fig. 20: CATHENA Prediction versus WL Experiment for 10-Fin Fuel

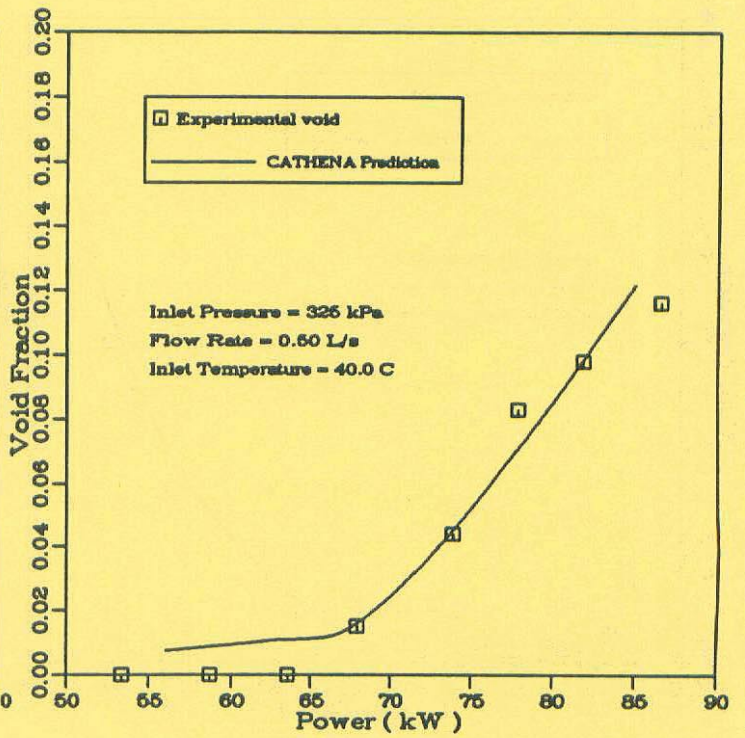


Fig. 22: CATHENA Prediction versus WL Experiment for 8-Fin Fuel

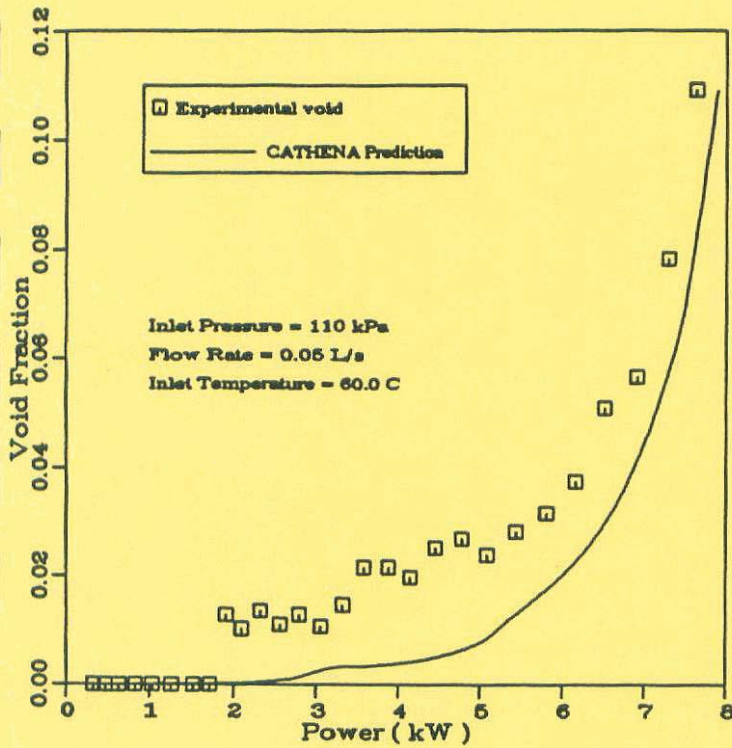


Fig. 23: CATHENA Prediction versus UBC Experiment for 8-Fin Fuel

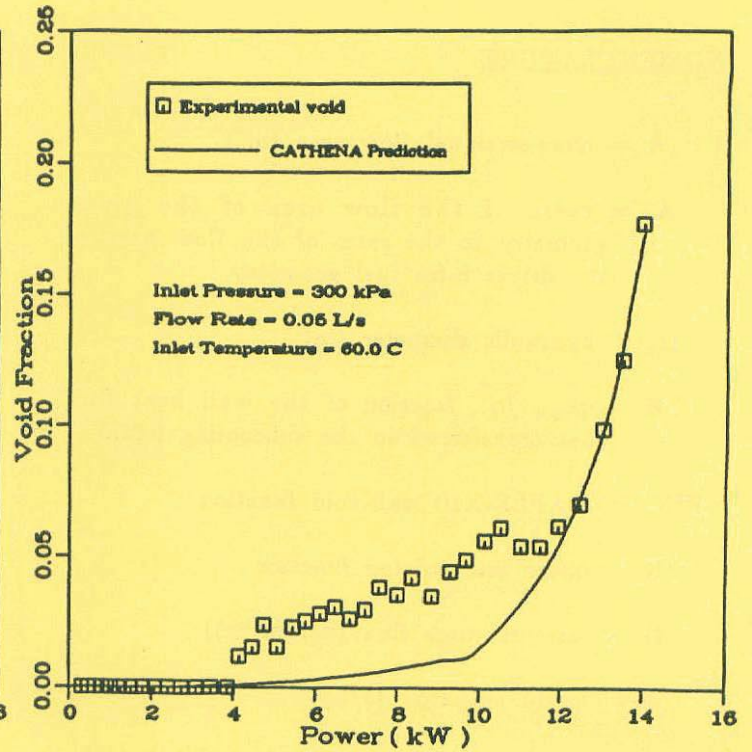


Fig. 25: CATHENA Prediction versus UBC Experiment for 8-Fin Fuel

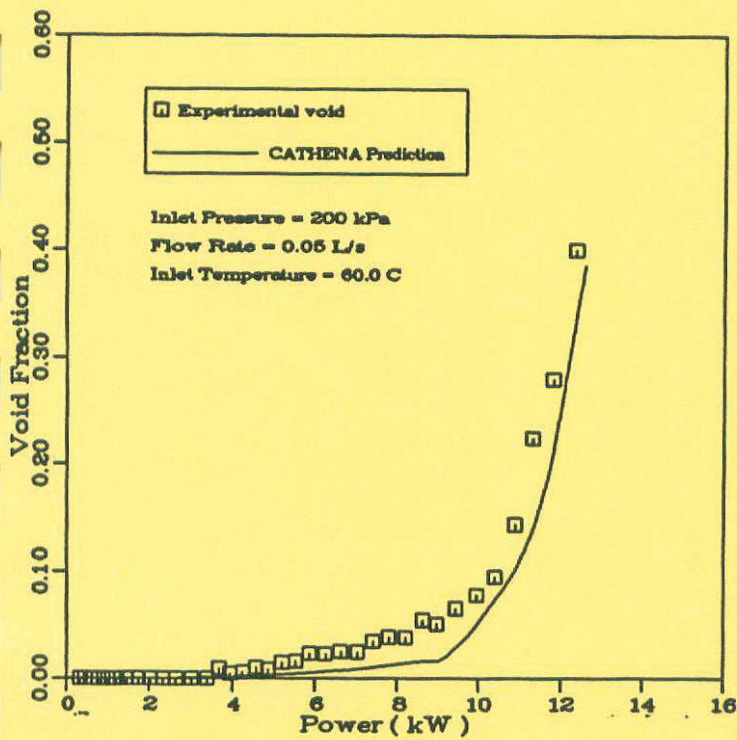


Fig. 24: CATHENA Prediction versus UBC Experiment for 8-Fin Fuel

NOMENCLATURE

A = cross-sectional flow area (m^2)

A_r = ratio of the flow area of the given geometry to the ratio of the flow area of the driver 8-fin fuel geometry

D_h = hydraulic diameter (m)

$FB = \bar{q}_{OSV} / \bar{q}$, fraction of the wall heat flux that transferred to the subcooling liquid

FNC = MAPLE-X10 wall-void function

FR = linear interpolated function

G = mixture mass flux ($\text{kg}/(\text{m}^2 \cdot \text{s})$)

h = liquid enthalpy (J/kg)

h_{fg} = latent heat of vapourization (J/kg)

h_{sat} = liquid enthalpy at saturation (J/kg)

$N_s = \text{maximum}(-x_{eq}, 0.005)$, subcooling number

P = pressure (N/m^2)

P_r = ratio of the fuel pin cross-sectional area to the reference fuel pin cross-sectional area

\bar{q} = wall heat flux (W/m^2)

\bar{q}_{ONB} = wall heat flux at ONB point (W/m^2)

\bar{q}_{OSV} = wall heat flux at OSV point (W/m^2)

r_d = average bubble radius at departure point (m)

$Re_b = G \cdot D_h / \mu$, Reynolds number evaluated at bulk condition

$x_{eq} = (h - h_{sat}) / h_{fg}$, thermal equilibrium quality

Greek Symbols

δ = average vapour thickness on the wall (m)

α_{OSV} = void fraction at OSV heat flux

α_w = void fraction in the wall-void region

μ = Liquid viscosity, ($\text{kg}/(\text{m} \cdot \text{s})$)